Mechanics of axisymmetric adhesive contact of rough surfaces involving power-law graded materials

Fan Jin, Xu Guo

PII: S0020-7683(13)00248-5
DOI: http://dx.doi.org/10.1016/j.ijsolstr.2013.06.007
Reference: SAS 8030

To appear in: *International Journal of Solids and Structures*

Received Date: 10 September 2012
Revised Date: 28 April 2013

Please cite this article as: Jin, F., Guo, X., Mechanics of axisymmetric adhesive contact of rough surfaces involving power-law graded materials, *International Journal of Solids and Structures* (2013), doi: http://dx.doi.org/10.1016/j.ijsolstr.2013.06.007

Mechanics of axisymmetric adhesive contact of rough surfaces involving power-law graded materials

Fan Jin Xu Guo*

State Key Laboratory of Structural Analysis for Industrial Equipment
Department of Engineering Mechanics
Dalian University of Technology, Dalian, 116023, P.R. China

Abstract: In the present paper, the mechanics of axisymmetric adhesive contact of rough surfaces involving power-law graded materials is investigated analytically. A series of general analytical solutions have been obtained with use of the cumulative superposition and equivalent energy release rate approaches. These solutions provide closed-form expressions of equilibrium relations among applied load, indentation depth and contact radius. Based on these solutions, an effective macroscopic description of the contact evolution is obtained for a general punch profile with surface roughness. Our analysis results reveal that the simultaneous presence of surface roughness and graded material properties can influence the pull-off force and energy dissipation due to adhesion hysteresis significantly. Moreover, it is found that both the adhesion strength and toughness can be optimized by adjusting the surface topography and material parameters of power-law graded solids appropriately. The analytical results obtained in this paper include the corresponding solutions for homogeneous isotropic materials as special cases and therefore can also serve as the benchmarks for checking the validity of numerical solution results.

Keywords: Contact mechanics; JKR model; Power-law graded materials; Surface roughness; Adhesion hysteresis

* Corresponding author guoxu@dlut.edu.cn; Tel: +86-411-84707807

1. Introduction

The effects of surface roughness on adhesion have attracted enormous attentions for their key role in many physical and biological systems (Persson, 2006; Jagota and Hui, 2011) in the last three decades. In parallel with the classical adhesion theories represented by JKR (Johnson et al., 1971), DMT (Derjaguin et al., 1975) and MD (Maugis, 1992) models, their counterparts involving random surface roughness have been proposed by Fuller and Tabor (1975), Maugis (2000) and Morrow et al. (2003), respectively. These works stem from the Greenwood-Williamson theory (1966) (a development of Zhuravlev's theory (2007)) where rough surfaces were modeled as an ensemble of non-interacting asperities with identical radius of curvature but Gaussian distributed heights. These asperity-type contact models all made the same conclusion that increasing roughness may result in a monotonic decrease of adhesion. This conclusion makes intuitive sense because roughened stiff surfaces do have the effect to prevent intimate contact. However, these models cannot explain the contradictory experimental evidence such that for some soft elastomeric materials, the adhesion may increase initially with surface roughness before eventually decreasing (Fuller and Roberts, 1981; Kim and Russell, 2001). Besides, the asperity geometry was predicted to have significant influence on the adhesive behaviors (Rabinovich et al., 2000; Galanov, 2011). On the other hand, one-length scale roughness was often represented by a sinusoidal wavy profile for exact analytic solutions in the periodic contact models (Johnson (1995), Hui et al. (2001)). It is founded that asperity interaction may cause the two elastic surfaces to jump into full contact from partial contact in the absence of external load.

Recently, Guduru (2007) developed a theoretical model with only a concentric circular contact region to study the JKR adhesion between an elastic half-space and a rigid parabolic punch with sinusoidal undulations. The surface waviness was found to render the decohesion process oscillatory with intrinsic instabilities, causing apparent interface strengthening in the form of higher pull-off force and

interface toughening by irreversible energy dissipation in the contact process. This theory was then validated by experiments performed on gelatin by Guduru and Bull (2007). Waters et al. (2009) proceeded further to extend this model to a more realistic case with JKR-DMT transition adhesion. More recently, Kesari et al. (2010) reported that adhesion hysteresis may exist even without moisture, plasticity and viscoelasticity but hinges solely on the surface roughness. To interpret the observed hysteresis phenomenon, an improved theoretical model based on Guduru's analytical solution was developed by Kesari and Lew (2011) to investigate the effective macroscopic adhesive contact behavior of contact systems with surface roughness. It was found that the macroscopic behavior curve predicted by their theoretical model matched the experiment data well and better estimates for material properties were obtained than the typical JKR formulations.

Most of the above mentioned works have focused on homogeneous isotropic elastic materials. On the other hand, the study of functionality graded materials (FGMs) has recently emerged as an important research topic in several communities because of their great potential applications in many physical and biological systems (Suresh, 2001, Sherge and Gorb, 2001). Even for smooth contact model, however, only few theoretical works on adhesive behavior of FGMs has been done for power-law graded pattern (Chen et al., 2009a, 2009b; Jin and Guo, 2010, 2012; Guo et al., 2011; Jin et al., 2013). Under this circumstance, understanding the adhesion behavior of contact systems with both surface roughness and nonhomogeneous materials remains to be a challenging topic. To our knowledge, there is still lack of a general analytical approach to quantify the role of surface roughness and the resulting hysteresis effect on the adhesive behavior of graded solids. Motivated by the works of Guduru (2007) and Kesari and Lew (2011) on homogeneous materials, the present paper aims at extending these solutions to the case of power-law graded elastic materials, with special emphasis on establishing an analytical approach and a set of analytical solutions to provided physical insights into the roughness strengthening and toughening

mechanisms in graded solids. These results also suggest strategies to control the interfacial adhesion strength and toughness by appropriate surface topography optimization and material selection.

The plan of the present paper is as follows. First, the considered model problem is described in section 2. As an application of the generalized cumulative superposition and an energy release rate approach, the Hertzian and JKR solutions for an arbitrary axisymmetric punch contacting with a power-law graded half-space are derived in section 3 and 4, respectively. In section 5, based on the results derived in previous sections, a series of closed-form analytical solutions are provided, including the equilibrium relations among applied load, indentation depth and contact radius. With use of these solutions, the asymptotic representation of the equilibrium curves as well as the effective macroscopic description of the contact evolutions, are also obtained for a general punch profile with surface roughness. In addition, as an illustrative example, an axisymmetric parabolic punch with sinusoidal roughness is analyzed in detail. The corresponding energy dissipation during a loading/unloading process is also discussed thoroughly in this section. Finally, some concluding remarks are provided in section 6.

2. Analysis model for adhesive contact with surface roughness

The model problem considered in the present study is illustrated schematically in Fig. 1, where an axisymmetric rigid punch with small surface roughness is in frictionless adhesive contact with a power-law graded half-space under a normal loading P ($P<0$ in the case of tensile force). A cylindrical coordinate system (r,z) is set up with origin at the contact center and z direction pointing into the half-space. Similar to Kesari and Lew (2011), the multiscale punch profile which accounts for both macroscale geometry of the punch and the microscale surface roughness can be expressed as

$$f(r) = f_1(r) + \lambda f_2(r/\lambda) \ . \qquad (2.1)$$

Here $f_1(r)(\geq 0)$, which measures the large-scale topography of the punch, is a monotonically increasing and differentiable function of radius r with $f_1(0) = df_1/dr|_{r=0} = 0$. In its undeformed configuration, the rough surface of the punch is described as a product of a length parameter λ and a smooth 1-periodic function $f_2(r/\lambda)$ with $f_2(0) = 0$. In the present study, it is assumed that λ is far smaller in comparison to the other length parameters so that multiple asperities can come into contact with the half-space.

Guduru (2007) pointed out that in order to avoid the appearance of multiply connected regions, a sufficient condition is such that $f(r)$ in Eq. (2.1) should be a monotonically increasing function with respect to r. This condition is, however, too restrictive to allow for the consideration of more general contact cases. In fact the necessary and sufficient condition guaranteeing the simply connectedness of contact region is that the z-displacement of the half-space (i.e., u_z) should be greater than the punch's profile, i.e.,

$$u_z(r) \geq \delta - f(r), \qquad r \geq a \qquad (2.2)$$

for all indentation depth δ. This condition must be respected in the corresponding theoretical analysis.

The graded half-space involved in the considered problem has a constant Poisson's ratio ν and a Young's modulus varied with depth according to a power-law form as

$$E = E_0(z/c_0)^k, \qquad 0 \leq k < 1, \qquad (2.3)$$

where E_0 is a reference modulus, $c_0 > 0$ is a characteristic depth and k is the gradient exponent. It is obvious that homogeneous isotropic material is recovered as $k = 0$ while the Gibson solid is obtained as $k = 1$ and $\nu = 0.5$.

In the following sections, we shall solve the above model problem based on a general solution procedure.

3. Generalized cumulative superposition method and Hertzian solutions

Cumulative superposition is a concise approach to determine the influence of punch profile on the contact behavior in the absence of adhesion without solving the field equations. The key idea of this approach is based on the fact that the punch indentation to any depth can be regarded as the accumulation of a series of small indentations corresponding to a flat-ended punch if the contact region is always simply connected (Hill and Storakers, 1990; Bower, 2006). Although initially developed for homogeneous materials without adhesion, this approach is in fact also valid when the adhesive contact behavior of power-law graded materials is considered. In the following, based on the generalized cumulative superposition and an energy release rate approaches, the Hertzian and JKR solutions for an arbitrary axisymmetric punch contacting with a power-law graded half-space will be presented. To this end, the results associated with the circular flat-ended cylinder are reviewed firstly.

3.1 Indentation of a power-law grade half-space by a circular flat-ended cylinder

When the half-space is made of power-law grade materials, Booker et al. (1985) and Giannakopoulos and Suresh (1997) obtained the corresponding Boussinesq contact solution for a circular flat-ended cylinder punch with radius a. In their solutions, the contact pressure distribution $p^*(r)$ and the z-displacement $w_z^*(r)$ of the half-space's outside the contact area are expressed in terms of indentation depth δ^* as

$$p^*(r) = \frac{\vartheta E^* \delta^*}{2^k \pi c_\delta^k} (a^2 - r^2)^{\frac{k-1}{2}}, \qquad r \le a \qquad (3.1)$$

and

$$u_z^r(r) = \frac{2\delta^r \cos\frac{k\pi}{2}}{\pi(1+k)}\left(\frac{a}{r}\right)^{1+k} {}_2F_1\left(\frac{1+k}{2}, \frac{1+k}{2}; \frac{3+k}{2}; \frac{a^2}{r^2}\right), \quad r \geq a, \qquad (3.2)$$

respectively. In Eqs. (3.1)-(3.2), ${}_2F_1$ represents Gauss's hypergeometric function, a is the radius of the cylinder and

$$\vartheta = \frac{2^{1+k}(1+k)\cos\frac{k\pi}{2}\Gamma\left(1+\frac{k}{2}\right)}{\sqrt{\pi}c\beta\sin\frac{\beta\pi}{2}\,\Gamma\left(\frac{1+k}{2}\right)}, \quad \beta = \sqrt{(1+k)\left(1-\frac{k\nu}{1-\nu}\right)},$$

$$E^r = \frac{E_0}{1-\nu^2}, \quad c = \frac{2^{1+k}\Gamma\left(\frac{3+k+\beta}{2}\right)\Gamma\left(\frac{3+k-\beta}{2}\right)}{\pi\Gamma(2+k)} \qquad (3.3)$$

with $\Gamma(\cdot)$ denoting the Gamma function. Note that $\vartheta = 1$ in the homogeneous limit of $k = 0$ while $\vartheta = \pi$ in the Gibson limit of $k = 1$ and $\nu = 0.5$. More general solutions for elasticity problems involving power-law grade materials can be found in Rvachev and Protsenko (1977).

3.2 Indentation by a rigid axisymmetric punch with an arbitrary profile

In the absence of adhesion, the Hertzian contact solution for a rigid axisymmetric punch with an arbitrary profile $f(r)$ can be obtained from the above fundamental solutions of flat-ended punch with use of the cumulative superposition approach (Mossakovskii, 1963).

Suppose that the indentation depth is increased by a small increment $\Delta\delta$ at a contact radius $(0 \leq r \leq a)$, then the normal surface displacement u_z and the contact pressure p will acquire a corresponding increment Δu_z and Δp, respectively. Since $\Delta u_z = \Delta\delta$ within the contact region, it is apparent that the

stress and displacement fields will be similar to those for a circular flat-ended cylinder. In view of this, $p(r)$ and $u_z(r)$ corresponding to any indentation depth can be obtained from the following integrations:

$$p(r) = \frac{\vartheta E^*}{2^k \pi c_\beta^k} \int_r^a \frac{\delta'(s)}{(s^2 - r^2)^{\frac{1-k}{2}}} \mathrm{d}s, \qquad r \le a, \qquad (3.4)$$

$$u_z(r) = \frac{2\cos\frac{k\pi}{2}}{\pi(1+k)} \int_0^a \left(\frac{s}{r}\right)^{1+k} \delta'(s)\, {}_2F_1\left(\frac{1+k}{2}, \frac{1+k}{2}; \frac{3+k}{2}; \frac{s^2}{r^2}\right) \mathrm{d}s$$

$$= \frac{2\cos\frac{k\pi}{2}}{\pi(1+k)} \left(\frac{a}{r}\right)^{1+k} \delta(a)\, {}_2F_1\left(\frac{1+k}{2}, \frac{1+k}{2}; \frac{3+k}{2}; \frac{a^2}{r^2}\right)$$

$$- \frac{2\cos\frac{k\pi}{2}}{\pi} \int_0^a \frac{s^k \delta(s)}{(r^2 - s^2)^{\frac{1-k}{2}}} \mathrm{d}s, \qquad r \ge a, \qquad (3.5)$$

where $\delta'(s) = \mathrm{d}\delta/\mathrm{d}s$. In particular, the z-displacement of half-space at the contact edge ($r = a$) can be expressed from Eq. (3.5) as

$$u_z(a) = \delta(a) - \frac{2\cos\frac{k\pi}{2}}{\pi} \int_0^a \frac{s^k \delta(s)}{(a^2 - s^2)^{\frac{1-k}{2}}} \mathrm{d}s. \qquad (3.6)$$

Since from the geometric relation

$$u_z(a) = \delta(a) - f(a), \qquad (3.7)$$

a comparison of Eq. (3.6) with Eq. (3.7) leads to the fact that

$$f(a) = \frac{2\cos\frac{k\pi}{2}}{\pi} \int_0^a \frac{s^k \delta(s)}{(a^2 - s^2)^{\frac{1-k}{2}}} \mathrm{d}s. \qquad (3.8)$$

Eq. (3.8) is a generalized Abel integral equation from which the indentation depth can be expressed in terms of f as (see Appendix A for details)

$$\delta(a) = a^{1-k} \int_0^a \frac{f'(s)}{(a^2 - s^2)^{\frac{1-k}{2}}} \mathrm{d}s, \qquad (3.9)$$

where $f'(s) = \mathrm{d}f/\mathrm{d}s$. In addition, the $P - \delta$ relation can be established from Eq. (3.4) as

$$P = 2\pi \int_0^a rp(r)dr = 2^{1-k}\vartheta \frac{E^*}{c_0^k}\left[\frac{a^{1+k}}{1+k}\delta(a) - \int_0^a \frac{sf(s)}{(a^2-s^2)^{\frac{1-k}{2}}}ds\right], \qquad (3.10)$$

Up to this point, the Hertzian contact solutions are available as long as the punch profile $f(r)$ is specified. It can also be verified that $u_z(r)$ and $\delta(a)$ obtained above does satisfy the simply-connected contact condition described in Eq. (2.2).

4. Extension to JKR-type adhesion

In this section, we shall make an extension of the above obtained Hertzian contact solutions to the case of JKR-type adhesion (Johnson et al., 1971). As pointed out by Johnson (1985) and Maugis (1992), in general, the adhesive contact solution can be constructed by superposing the corresponding Hertzian solution of a punch with the same profile and that of a flat-ended cylinder punch. Based on this argument, the following relations can be established:

$$\delta = \delta_H - \frac{1+k}{2^{1-k}\vartheta}\frac{c_0^k}{E^* a^{1+k}}(P_H - P), \qquad (4.1)$$

$$p(r) = p_H(r) - \frac{(1+k)(P_H - P)}{2\pi a^2}\left[1 - \left(\frac{r}{a}\right)^2\right]^{\frac{k-1}{2}}, \qquad r \le a, \qquad (4.2)$$

$$u_z(r) = u_z^H(r) - (P_H - P)\frac{2^k c_0^k \cos\left(\frac{k\pi}{2}\right)}{\pi\vartheta E^* r^{1+k}}\,{}_2F_1\left(\frac{1+k}{2}, \frac{1+k}{2}; \frac{3+k}{2}; \frac{a^2}{r^2}\right), \quad r \ge a, \qquad (4.3)$$

where δ_H, P_H, $p_H(r)$ and $u_z^H(r)$ are the Hertzian solutions given in Eqs. (3.9), (3.10), (3.4) and (3.5), respectively. With use of the Griffith's energy balance principle, the following identity can be established (Jin and Guo, 2012)

$$G = \frac{K_I^2}{2M} = \Delta\gamma, \qquad (4.4)$$

where

$$K_I = \sqrt{2\pi}\lim_{r\to a}(a-r)^{\frac{1-k}{2}}p(r) = -\frac{(1+k)(P_H-P)}{2^{\frac{1-k}{2}}\sqrt{\pi a}^{\frac{3-k}{2}}}, \qquad (4.5)$$

$$M = \vartheta E^*/c_\beta^k \qquad (4.6)$$

and $\Delta\gamma$ denotes the surface energy which is taken to be the work of adhesion in the absence of energy dissipation. Combining Eqs. (4.4)-(4.6) gives rise to the following $P-a$ relation:

$$P = P_H - \sqrt{\frac{2^{3-k}\pi\vartheta}{(1+k)^2}\frac{E^*\Delta\gamma a^{3+k}}{c_\beta^k}}. \qquad (4.7)$$

Inserting Eq. (4.7) back into Eqs.(4.1)-(4.3) yields the whole set of JKR-type solutions:

$$\delta = \delta_H - \sqrt{2^{1+k}\pi\Delta\gamma\frac{c_\beta^k a^{1-k}}{\vartheta E^*}}, \qquad (4.8)$$

$$p(r) = p_H(r) - \sqrt{2^{1-k}\vartheta\frac{E^*\Delta\gamma}{\pi c_\beta^k}}(a^2-r^2)^{\frac{k-1}{2}}, \quad r \le a, \qquad (4.9)$$

$$u_z(r) = u_z^H(r) - \sqrt{\frac{2^{3+k}a^{3+k}c_\beta^k\Delta\gamma\cos\left(\frac{k\pi}{2}\right)}{(1+k)^2\pi\vartheta E^*}}\frac{}{r^{1+k}}\,{}_2F_1\left(\frac{1+k}{2},\frac{1+k}{2},\frac{3+k}{2},\frac{a^2}{r^2}\right),$$

$$r \ge a. \qquad (4.10)$$

It can be observed from the above equations that the effect of the punch profile is only embodied in the part of Hertzian solutions. Moreover, the simply connected contact condition described in Eq. (2.2) needs to be checked a posteriori to verify that the contact area is indeed a circular one as assumed from the beginning.

In the present paper, frictionless contact is assumed in the analysis model. Another situation which may be of great concern in real applications is the non-slipping case with a perfectly bonded contact interface. In the absence of surface roughness, as shown by Guo et al. (2011), the frictionless JKR-type solution obtained here still applies strictly for non-slipping contact on homogeneous incompressible solids and linearly graded power-law materials.

However, for general soft compressible materials, the non-slipping interface condition tends to reduce both the contact area and the indentation depth. The effect of surface roughness on adhesion behavior under non-slipping case will be the subject of a separate work.

5. Solutions to a punch with surface roughness

5.1 Equilibrium equations

For the adhesive contact problem described in section 2, one of our main concerns is the equilibrium relations among applied load, indentation depth and contact radius. Inserting the punch profile $f(r)$ prescribed in Eq. (2.1) into Eqs. (3.9)-(3.10) and then into Eqs. (4.8)-(4.7) leads to JKR solutions as

$$\delta(a) = \delta_L(a) + a^{1-k}\int_0^a \frac{f_s'(s/\lambda)}{(a^2-s^2)^{\frac{1-k}{2}}}\mathrm{d}s\,, \tag{5.1}$$

$$P(a) = P_L(a) + \frac{2^{1-k}\vartheta E^*}{(1+k)c_\beta^k}\left[a^2\int_0^a \frac{f_s'(s/\lambda)}{(a^2-s^2)^{\frac{1-k}{2}}}\mathrm{d}s - \int_0^a (a^2-s^2)^{\frac{1+k}{2}} f_s''\left(\frac{s}{\lambda}\right)\mathrm{d}s\right], \tag{5.2}$$

where $f_s'(s/\lambda)$ denotes the derivative with respect to s/λ and

$$\delta_L(a) = a^{1-k}\int_0^a \frac{f_1'(s)}{(a^2-s^2)^{\frac{1-k}{2}}}\mathrm{d}s - \sqrt{2^{1+k}\pi\Delta\gamma\frac{c_\beta^k a^{1-k}}{\vartheta E^*}}\,, \tag{5.3}$$

$$P_L(a) = \frac{2^{1-k}\vartheta E^*}{(1+k)c_\beta^k}\left[a^{1+k}\delta_L(a) - \int_0^a (a^2-s^2)^{\frac{1+k}{2}} f_1''(s)\mathrm{d}s\right]. \tag{5.4}$$

In the absence of small surface roughness, if the large-scale topography of the punch is of polynomial form $f_1(r) = r^m/mR^{m-1}$ with an index $m \geq 1$ and a characteristic length $R > 0$, the equilibrium $P_L - \delta_L$ curve behaves as

$$\delta_L(a) = \frac{\Gamma(m/2)\Gamma(1/2+k/2)}{2\Gamma(1/2+m/2+k/2)}\frac{a^m}{R^{m-1}} - \sqrt{2^{1+k}\pi\Delta\gamma\frac{c_\beta^k a^{1-k}}{\vartheta E^*}}\,, \tag{5.5}$$

$$P_L(a) = \frac{2^{1-k}\vartheta E^*}{(1+k)c_\beta^k}\left[a^{1+k}\delta_L(a) - \frac{\Gamma(m/2)\Gamma(3/2+k/2)}{2\Gamma(3/2+m/2+k/2)}\frac{a^{1+k+m}}{R^{m-1}}\right]. \tag{5.6}$$

As expected, in the homogeneous limit ($k = 0$), δ_L and P_L reduce to the results given by Borodich (2008). Besides, the JKR solutions for power-law graded solids under a parabolic punch profile can be recovered by letting $m = 2$ in Eqs. (5.5)-(5.6) (Chen et al., 2009b).

To make the discussions more concrete, in the following, we shall focus on a specified punch profile which is a parabolic function with a single wavelength sinusoidal undulation of small amplitude, that is

$$f_1(r) = \frac{r^2}{2R}, \qquad f_2\left(\frac{r}{\lambda}\right) = A\left(1 - \cos\frac{2\pi r}{\lambda}\right), \tag{5.7}$$

where A is a positive non-dimensional parameter which measures the ratio of the wave amplitude to the wavelength λ. Inserting Eq. (5.7) into Eqs. (5.1)-(5.4) leads to the equilibrium $P - \delta$ curve as

$$\delta(a) = \delta_L(a) + \lambda A\sqrt{\pi}\Gamma\left(\frac{1+k}{2}\right)\left(\frac{\pi a}{\lambda}\right)^{1-\frac{k}{2}} H_{\frac{k}{2}}\left(\frac{2\pi a}{\lambda}\right), \tag{5.8}$$

$$P(a) = P_L(a) + \frac{\left(2\sqrt{\pi}\right)^{1-k}\vartheta E^*}{(1+k)c_\beta^k} A(\lambda a)^{\frac{k}{2}}$$

$$\times\left[\pi a^2\Gamma\left(\frac{1+k}{2}\right)H_{\frac{k}{2}}\left(\frac{2\pi a}{\lambda}\right) - \lambda a\Gamma\left(\frac{3+k}{2}\right)H_{1+\frac{k}{2}}\left(\frac{2\pi a}{\lambda}\right)\right], \tag{5.9}$$

where $H_\nu(\cdot)$ represents the ν-th Struve function and

$$\delta_L(a) = \frac{1}{1+k}\frac{a^2}{R} - \sqrt{2^{1+k}\pi\Delta\gamma\frac{c_\beta^k a^{1-k}}{\vartheta E^*}}, \tag{5.10}$$

$$P_L(a) = \frac{2^{3-k}\vartheta}{(1+k)^2(3+k)}\frac{E^* a^{3+k}}{c_\beta^k R} - \sqrt{\frac{2^{3-k}\vartheta\pi}{(1+k)^2}\frac{E^*\Delta\gamma a^{3+k}}{c_\beta^k}}. \tag{5.11}$$

In the homogeneous limit ($k \to 0$), the corresponding equilibrium $P - \delta$ curve for homogeneous isotropic materials, which was first obtained by Guduru (2007), is recovered from Eqs. (5.8)-(5.11).

Evolutions of the equilibrium $P - \delta$ curve for $k = 0.1$ and $k = 0$ are

shown in Fig. 2a-2b according to Eqs. (5.8)-(5.11), respectively. In this plot, the parameters are selected to satisfy the simply connected condition in Eq. (2.2). The equilibrium curves for graded materials and homogeneous solids are qualitatively similar and the latter case has been discussed intensively by Guduru (2007) and Kesari and Lew (2011). In contrast to its smooth counterpart without surface roughness (pink solid line), the equilibrium $P-\delta$ relation with surface roughness exhibits many corrugations between alternating stable (black dashed line) and unstable segments (black solid line). Another distinctive feature in the presence of surface roughness is such that for every fixed value of δ, the corresponding equilibrium normal force P is non-unique but has multiple values. In essence, this phenomenon results from the fact that a prescribed indentation depth may correspond to several locally stable contact configurations when surface roughness exists. However, the actual equilibrium path taken by the contact system may not follow the folds on the $P-\delta$ curve. As pointed out by Kesari and Lew (2011), the contact system may experience snap-through at some critical points where the original equilibrium path becomes unstable and then reestablish a new equilibrium state, which always corresponds to the first neighboring local minimizer of the potential energy of the system.

To illustrate this point of view more explicitly, Figs. 3a-c plot the actual path taken by the contact system under a displacement controlled mode in $P-\delta$, $\delta-a$ and $P-a$ spaces, respectively. In Figs. 3a-c the corresponding points in different parameter spaces are labeled with the same letter. For the considered case, as shown in Fig. 3a, the contact system is first loaded to the maximum indentation depth δ_{max} (point G) and then unloaded until pull-off occurs (point K). The pull-off force is quantified by the most negative value of P corresponding to point J in the figures. It can be seen from these figures that the

actually path is only parts of the equilibrium curves (red solid line) combined with unstable jumps at the tip of each corrugation (red dashed line). These unstable jumps include A→B, C→D, E→F during loading stage and H→I, K→L during unloading stage, where the abrupt contact (A→B) and separation (K→L) are known as jump-in (pull-in) and jump-out (pull-off) instabilities, respectively. It is at the point F that the loading and unloading stages begin to differ. The different paths of the loading and unloading stages induced by the surface roughness compose a loop whose area quantifies the energy loss during the deformation process, which is directly dependent on the maximum indentation depth δ_{max}. In view of this, this energy dissipation mechanism is also referred as (indentation) Depth-Dependent Hysteresis (DDH) due to surface roughness. The DDH phenomenon for power-law graded material is qualitatively similar to that for homogeneous isotropic material, which has been systematic illustrated by Kesari and Lew (2011).

The pull-off force is characterized by the most negative value of P on the $P-\delta$ curve (i.e., $F_{pf}=-P_{min}$). For the case of homogeneous materials, under the assumption such that initially intimate contact is maintained before detachment, Guduru (2007) pointed out that the normalized pull-off force $\bar{F}_{pf}=(-P_{min})/1.5\pi R\Delta\gamma$ is dependent on four non-dimensional parameters including A, $E^*R/\Delta\gamma$, λ/R and a_{max}/R with a_{max} denoting the characteristic size of the punch and the magnitude of $\bar{F}_{pf}$ can be amplified significantly by introducing surface waviness. In the present study, it is found that for the considered power-law graded materials besides the above four parameters, two additional quantities i.e., the gradient exponent k and the non-dimensional

modulus variation rate c_0/R will come into play. The effects of k and c_0/R on the $\bar{F}_{pf} - \lambda_f/R$ relation are shown in Fig. 4a and Fig. 4b, respectively. An interesting observation from Fig. 4a is that the maximum value of the pull-off force is not a monotonic function of k. There exists an optimal value of $k = k_{opt}$ ($k_{opt} \approx 0.7$ for the considered case) at which the strongest adhesion (measured in terms of pull-off force) can be achieved by selecting the surface waviness appropriately. Our analysis also indicates that the modulus variation rate c_0/R of the power-law graded material also has a significant influence on the adhesion strength. As shown in Fig. 4b, the maximum value of the pull-off force increases as c_0/R decreases. This is quite different from the case of smooth contact, where the pull-off force is irrespective of c_0/R (Chen et al., 2009b). Consequently, it is feasible that interface adhesion strength can be optimized by adjusting both the surface topography and the material parameters of the graded solids appropriately.

The above analysis is performed under the assumption that the in-plane size of the punch is large enough. This is, however, not always valid in practice. The effect of the finite punch size on the pull-off force is plotted in Fig. 4c by truncating the abscissa of the corresponding $\bar{F}_{pf} - a/R$ at different values of a_{max}/R and selecting the most negative values in the interval of $(0, a_{max}/R)$. An obvious message from this figure is that the global maximum pull-off force will decrease and more local maxima will be introduced when the in-plane size of the punch becomes finite, which is qualitatively the same as in the case of homogeneous materials (Guduru, 2007). Furthermore, it is also found that $a_{max}/R \approx 0.56$ is a threshold beyond which the behaviors of the finite and

infinite size punch are exactly the same.

5.2 Asymptotic form

For most engineered surfaces, modern technology can now make it possible to restrict the value of λ below a certain length scale which is far smaller in comparison to the other physical dimensions of the contact system. Under this circumstance, the asymptotic form of the equilibrium $P-\delta$ curve in the limit of $\lambda/a \to 0$ is of special interest. In the following, this point will be discussed in details.

As $f_s(\xi)$ is a smooth periodic function with period 1, its Fourier series can then be expressed as

$$f_s(\xi) = \frac{a_0}{2} + \sum_{n=1}^{\infty}[a_n \cos(2n\pi\xi) + b_n \sin(2n\pi\xi)], \qquad (5.12)$$

where

$$a_n = 2\int_{-1/2}^{1/2} f_s(\xi)\cos(2n\pi\xi)\,d\xi, \quad n \geq 0, \qquad (5.13)$$

$$b_n = 2\int_{-1/2}^{1/2} f_s(\xi)\sin(2n\pi\xi)\,d\xi, \quad n \geq 1. \qquad (5.14)$$

As $\lambda/a \to 0$, the origin equilibrium $P-\delta$ curve in Eqs. (5.1)-(5.2) behaves in a simple asymptotic form as (see Appendix B for more details)

$$\delta(a) \sim \delta_L(a) + 2^{\frac{k-1}{2}} a^{\frac{1-k}{2}} \Gamma\left(\frac{1+k}{2}\right) \lambda^{\frac{1+k}{2}} \varsigma\left(\frac{a}{\lambda}\right), \qquad (5.15)$$

$$P(a) \sim P_L(a) + \frac{2^{\frac{1-k}{2}} \vartheta E^*}{(1+k)c_k^{\frac{1+k}{2}}} \Gamma\left(\frac{1+k}{2}\right) \lambda^{\frac{1+k}{2}} a^{\frac{3+k}{2}} \varsigma\left(\frac{a}{\lambda}\right), \qquad (5.16)$$

where

$$\varsigma(\xi) = \sum_{n=1}^{\infty} (2\pi n)^{\frac{1-k}{2}} \left[-a_n \sin\left(2n\pi\xi - \frac{k\pi}{4} - \frac{\pi}{4}\right) + b_n \cos\left(2n\pi\xi - \frac{k\pi}{4} - \frac{\pi}{4}\right)\right], \qquad (5.17)$$

Note that $\varsigma(\xi)$ is also a smooth periodic function with period 1 and it is actually the $(1-k)/2$-fractional derivative of $(f_s(\xi)-a_0/2)$ (Appendix B).

For the parabolic punch with sinusoidal roughness described in Eq. (5.7), after the substitution of Eq. (5.7) into Eqs. (5.12)-(5.17), the asymptotic form of the equilibrium $P-\delta$ curve in the limit of $\lambda/a \to 0$ can be approximated as

$$\delta(a) \sim \delta_L + 2^{\frac{k-1}{2}} a^{\frac{1-k}{2}} \Gamma\left(\frac{1+k}{2}\right) \lambda^{\frac{1+k}{2}} \varsigma\left(\frac{a}{\lambda}\right), \tag{5.18}$$

$$P(a) \sim P_L + \frac{2^{\frac{1-k}{2}} \vartheta E^*}{(1+k)c_k^k} \Gamma\left(\frac{1+k}{2}\right) \lambda^{\frac{1+k}{2}} a^{\frac{3+k}{2}} \varsigma\left(\frac{a}{\lambda}\right), \tag{5.19}$$

where

$$\varsigma(\xi) = (2\pi)^{\frac{1-k}{2}} A \sin\left(2\pi\xi - \frac{k\pi}{4} - \frac{\pi}{4}\right). \tag{5.20}$$

A comparison between the equilibrium $P-\delta$ curve (blue dashed line) and its asymptotic form (red solid line) is shown in Figs. 5a-c for different values of λ/R. The curves are obtained from the example in Fig. 2a and the asymptotic values are calculated from Eqs. (5.18)-(5.19). From these figures, it can be concluded that the asymptotic form can be used as a good approximation of the equilibrium curves for small roughness periodicity.

5.3 Approximate envelops and effective contact evolution path during early unloading

As shown in Fig. 3a, in a displacement controlled loading/unloading process, the contact system with surface roughness tends to find the most locally stable configuration under a given indentation-depth. Under this circumstance, by replacing the oscillatory terms in the asymptotic equation (5.18)-(5.19) with their respective maximum and minimum values, the approximate envelops of the equilibrium equations (5.1)-(5.2) can be defined as

$$\delta^{+}(a) \sim \delta_L - 2^{\frac{k-1}{2}} a^{\frac{1-k}{2}} \Gamma\left(\frac{1+k}{2}\right) \lambda^{\frac{1+k}{2}} \varsigma^{+} , \qquad (5.21)$$

$$P^{+}(a) \sim P_L - \frac{2^{\frac{1-k}{2}} \vartheta E^{*}}{(1+k) c_\beta^k} \Gamma\left(\frac{1+k}{2}\right) \lambda^{\frac{1+k}{2}} a^{\frac{3+k}{2}} \varsigma^{+} , \qquad (5.22)$$

and

$$\delta^{-}(a) \sim \delta_L + 2^{\frac{k-1}{2}} a^{\frac{1-k}{2}} \Gamma\left(\frac{1+k}{2}\right) \lambda^{\frac{1+k}{2}} \varsigma^{-} , \qquad (5.23)$$

$$P^{-}(a) \sim P_L + \frac{2^{\frac{1-k}{2}} \vartheta E^{*}}{(1+k) c_\beta^k} \Gamma\left(\frac{1+k}{2}\right) \lambda^{\frac{1+k}{2}} a^{\frac{3+k}{2}} \varsigma^{-} , \qquad (5.24)$$

where

$$\varsigma^{+} = -\max_{\xi} \varsigma(\xi) \leq 0 , \qquad \varsigma^{-} = \min_{\xi} \varsigma(\xi) \leq 0 \qquad (5.25)$$

and the $\pm$ signs denote the loading and unloading phases of the process, respectively. Note that when $\varsigma = 0$ both the loading and unloading branches collapse to a single curve, which is in agreement with the corresponding smooth adhesion for power-law graded materials with a punch profile $f_1(r)$.

For the parabolic punch with sinusoidal roughness described in Eq. (5.7), inserting Eq. (5.7) into Eqs. (5.21)-(5.25) leads to the approximate envelops as

$$\delta \approx \sim \frac{1}{1+k} \frac{a^2}{R} - \sqrt{2^{1+k} \pi \Delta\gamma \frac{c_\beta^k a^{1-k}}{\vartheta E^{*}}} \pm \pi^{\frac{1-k}{2}} \Gamma\left(\frac{1+k}{2}\right) A \lambda^{\frac{1+k}{2}} a^{\frac{1-k}{2}} , \qquad (5.26)$$

$$P \approx \sim \frac{2^{2-k}\vartheta}{(1+k)^2(3+k)} \frac{E^{*} a^{3+k}}{c_\beta^k R} - \sqrt{\frac{2^{3-k}\vartheta\pi}{(1+k)^2} \frac{E^{*} \Delta\gamma a^{3+k}}{c_\beta^k}}$$

$$\pm \frac{2^{1-k}\vartheta}{1+k} \pi^{\frac{1-k}{2}} \Gamma\left(\frac{1+k}{2}\right) A \frac{E^{*}}{c_\beta^k} \lambda^{\frac{1+k}{2}} a^{\frac{3+k}{2}} , \qquad (5.27)$$

Also, in the absence of surface roughness (i.e., $A = 0$), the loading and unloading branches reduce to a single curve, which corresponds to the JKR solution for power-law graded materials.

The envelop curve according to Eqs. (5.26)-(5.27) (green line) is shown in

Fig. 6, where the equilibrium $P-\delta$ curve (grey line) and the actual path (red line) are obtained from Fig. 3a. Slight discrepancy is observed between the envelop curve and the tips of each corrugation in the actual equilibrium curve. Strictly speaking, this envelop will reduce to the asymptotic equilibrium curve as $\lambda \to 0$ but only be approximated for any $\lambda \gg 0$.

The approximate envelops are completed by the early unloading stage approximation labeled by olive line in Fig. 6. For the actual $P-\delta$ curve, the indentation depth reaches the maximum value (i.e., δ_{max}) at point G, where the contact radius also reaches its maximum value simultaneously (i.e., $\delta(a_{max}) = \delta_{max}$). The segment G→H is the exact evolution path at initial unloading stage. Under this circumstance, the *approximate* maximum contact radius a_{am} can be calculated from the $\delta^* - a$ relation implicitly as $\bar{\delta}^*(a_{am}) = \delta_{max}$. As an approximation of the GH curve, the effective evolution path during the initial unloading stage in $\delta - a$ and $P - a$ spaces can be expressed approximately according to Eqs. (5.23)-(5.24) as

$$\delta^*(a) \sim \delta_L(a_{am}) + 2^{\frac{k-1}{k}} a_{am}^{\frac{2-k}{k}} \Gamma\left(\frac{1+k}{2}\right) \lambda^{\frac{1+k}{k}} a \,, \qquad (5.28)$$

$$P^*(a) \sim P_L(a_{am}) + \frac{2^{\frac{1-k}{k}} \vartheta E^*}{(1+k)c_k^{\frac{1}{k}}} \Gamma\left(\frac{1+k}{2}\right) \lambda^{\frac{1+k}{k}} a_{am}^{\frac{2+k}{k}} a \,, \qquad (5.29)$$

where $\zeta^- \le a \le -\zeta^+$. Since the range of the contact radius during initial unloading is within a segment lying between two consecutive tips of corrugation, the corresponding $P-\delta$ curve can be explicitly rewritten from Eqs. (5.28)-(5.29) as

$$P^*(\delta^*) \sim P_L(a_{am}) + \frac{2^{1-k} \vartheta E^*}{(1+k)c_k^{\frac{1}{k}}} a_{am}^{1+k} [\delta^* - \delta_L(a_{am})] \,, \qquad (5.30)$$

with $\delta_{max}^- \le \delta^* \le \delta_{max}$, where $\delta_{max}^- = \delta^-(a_{am})$ is obtained from

$$\bar{\delta}_{max}^{-} = \bar{\delta}_{max} + 2^{\frac{k-1}{k}} a_{am}^{\frac{1-k}{k}} \Gamma\left(\frac{1+k}{2}\right) \lambda^{\frac{1+k}{k}} (\zeta^{+} + \zeta^{-}) . \qquad (5.31)$$

For the parabolic punch with sinusoidal roughness described in Eq. (5.7), substitution of Eqs. (5.10)-(5.11) into Eq. (5.30) yields the effective evolution path during the early unloading stage as

$$P^{*}(\bar{\delta}^{*}) \sim \frac{2^{1-k} \vartheta E^{*}}{(1+k) c_{\beta}^{k}} a_{am}^{1+k} \bar{\delta}^{*} - \frac{2^{1-k} \vartheta E^{*} a_{am}^{3+k}}{(1+k)(3+k) c_{\beta}^{k} R} , \qquad (5.32)$$

for $\bar{\delta}_{max}^{-} \leq \bar{\delta}^{*} \leq \bar{\delta}_{max}$ with

$$\bar{\delta}_{max}^{-} = \bar{\delta}_{max} - 2\pi^{\frac{1-k}{k}} A \Gamma\left(\frac{1+k}{2}\right) \lambda^{\frac{1+k}{k}} a_{am}^{\frac{1-k}{k}} . \qquad (5.33)$$

Consequently, an effective macroscopic description of the response of the contact system for small λ can be obtained by combining envelops of the asymptotic equilibrium curve and the approximate curve during the initial unloading stage. As pointed by Kesari (Kesari et al., 2010; Kesari and Lew, 2011), the simpler effective macroscopic contact evolution curve can be used to estimate the material properties such as material stiffness and surface energy by fitting experiment data displaying adhesion hysteresis.

A comprehensive comparison between the effective and the actual evolution curves in a displacement controlled process for $P - \bar{\delta}$, $\bar{\delta} - a$ and $P - a$ are shown in Figs. 7a-c, respectively. The effective evolution curves ($P^{\pm}(a_{ap}^{\pm}(\bar{\delta}))$, $a_{ap}^{\pm}(\bar{\delta})$, and $P^{\pm}(a_{ap}^{\pm})$) labeled in green do not display the oscillations in the actual curves ($P^{\pm}(a^{\pm}(\delta))$, $a^{\pm}(\delta)$ and $P^{\pm}(a^{\pm})$) labeled in red. At the maximum indentation depth $\bar{\delta}_{max}$, the maximum contact radius in approximate and actual curves are a_{am} and a_{max}, respectively. At the instant of jump out, the minimum indentation depths (negative) in the effective and actual curves are $\bar{\delta}_{min}^{ap}$ and

δ_{min}, respectively. It is expected that the discrepancies between a_{am} and a_{max} as well as δ_{min}^{ap} and δ_{min} will become small enough and therefore can be neglected as $\lambda/a \to 0$.

5.4 Energy loss during a displacement controlled contact process

As shown above, different branches of the equilibrium path in the loading and unloading phases induced by surface roughness will form a hysteretic loop, which may lead to an irreversible energy dissipation quantified by its enclose area. In fact, adhesion hysteresis and the corresponding energy loss have been found to be a common feature in rough surface adhesion (Goryacheva and Makhovskaya, 2004; Zappone et al., 2007; Li and Kim, 2009; Wei et al., 2010; Kesari et al., 2010). In this section we shall derive an approximate analytical expression of the energy loss $\mathcal{H}$ in terms of the maximum approximate contact radius a_{am} and other material parameters. To be specific, a parabolic punch with sinusoidal undulation given by Eq. (5.7) in a hypothetical displacement controlled experiment will be considered.

Fig. 8 shows the asymptotic $P-\delta$ curve described by Eqs. (5.18)-(5.19) (grey line) and the corresponding effective evolution described by Eqs. (5.26)-(5.27) and Eq. (5.32) (green line). Starting at point 1, the punch abruptly jumps into point 2 with an initial contact radius a_2, and then the punch is loaded until the contact radius reaches the approximate maximum value a_{am} corresponding to point 3. After this, the punch is unloaded to point 4 with a contact radius a_4 followed by a jump-out instability. The curves labeled by 2-3 and 3'-4 evolve along the approximate envelops during loading and unloading stages according to Eq. (5.26) and Eq. (5.27), respectively. Moreover, the curve 3-3' behaves along the effective evolution path during early unloading stage

according to Eqs. (5.32), which also holds true for curve 2-2' with a_{am} replaced by a_2.

Before proceeding, it is of assistance to compute a_2 and a_4. Employing the identity $\delta^*(a_2) = 0$ in Eq. (5.26) gives rise to

$$a_2 = \left[(1+k)\left(\sqrt{2^{1+k}\pi\frac{c_0^{2k}\Delta\gamma R^2}{\vartheta E^*}} - \Gamma\left(\frac{1+k}{2}\right)\pi^{\frac{1-k}{2}}AR\lambda^{\frac{1+k}{2}}\right)\right]^{\frac{2}{2+k}}. \quad (5.34)$$

By solving $d\delta^*(a_4)/da = 0$ in Eq. (5.26), one obtains

$$a_4 = \left[\frac{1-k^2}{4}\left(\sqrt{2^{1+k}\pi\Delta\gamma\frac{c_0^{2k}R^2}{\vartheta E^*}} + \Gamma\left(\frac{1+k}{2}\right)\pi^{\frac{1-k}{2}}AR\lambda^{\frac{1+k}{2}}\right)\right]^{\frac{2}{2+k}}. \quad (5.35)$$

The area enclosed is split into two closed path C_1 and C_2, which gives the energy loss as

$$\mathcal{H} = \int_{C_1} P\,d\delta + \int_{C_2} P\,d\delta, \quad (5.36)$$

where

$$\int_{C_1} P\,d\delta = \int_{2'2} P\,d\delta + \int_{2'4} P\,d\delta, \quad (5.37)$$

$$\int_{C_2} P\,d\delta = \int_{40} P\,d\delta + \int_{02} P\,d\delta + \int_{23} P\,d\delta + \int_{32'} P\,d\delta. \quad (5.38)$$

In the simplification of Eq. (5.37), the facts that $P = 0$ in segment 0-1 together with $d\delta = 0$ in segments 4-0 and 1-2 have been used.

Evaluating the integrals over C_1 and expanding it around $\lambda = 0$ yields

$$\int_{C_1} P\,d\delta = F_0(k)\left(\frac{c_0^{2k}\Delta\gamma^{2-k}R^4}{\vartheta^2 E^{*2}}\right)^{\frac{1}{2+k}} + F_1(k)A\lambda^{\frac{1+k}{2}}\left(\frac{c_0^{k(1-k)}\Delta\gamma^{2-k}R^3}{\vartheta^{1-k}E^{*1-k}}\right)^{\frac{1}{2(2+k)}}$$
$$+O(\lambda^{1+k}), \quad (5.39)$$

where

$$F_0(k) \approx 7.1 + 9.1k - 1.4k^2 \ , \qquad (5.40)$$

$$F_1(k) \approx 29.6 - 23.6k + 6.5k^2 \ . \qquad (5.41)$$

Evaluating the integrals over C_2 leads to

$$\int_{C_2} P\,d\delta = A\Gamma\left(\frac{1+k}{2}\right)\sqrt{2^{3-k}\pi^{2-k}\lambda^{1+k}\Delta\gamma\frac{\vartheta E^*}{c_0^k}}\left(a_{am}^2 - a_2^2\right) \ . \qquad (5.42)$$

As a result, the total energy dissipated during a loading/unloading cycle can be expressed as

$$\mathcal{H} = F_0(k)\left(\frac{c_0^{2k}\Delta\gamma^{2-k}R^k}{\vartheta^2 E^{*2}}\right)^{\frac{1}{3-k}} + F_1(k)A\lambda^{\frac{1+k}{2}}\left(\frac{c_0^{k(1-k)}\Delta\gamma^{1-k}R^k}{\vartheta^{1-k}E^{*1-k}}\right)^{\frac{1}{2(3-k)}}$$
$$+A\Gamma\left(\frac{1+k}{2}\right)\sqrt{2^{3-k}\pi^{2-k}\lambda^{1+k}\Delta\gamma\frac{\vartheta E^*}{c_0^k}}\left(a_{am}^2 - a_2^2\right) + O\left(\lambda^{\frac{1+k}{2}}\right) \ . \qquad (5.43)$$

Fig. 9 shows the normalized energy dissipation $\mathcal{H}/R^2\Delta\gamma$ as a function of the gradient exponent k under different values of A and λ. In this plot, we set $a_{am} = 2a_2$ and other parameters are selected here to satisfy the simply connected condition. The curve corresponding to $A = 0$ or $\lambda = 0$ evolves according to the first term in the right hand side of Eq. (5.43), which quantifies the energy loss solely induced by the jump-in and jump-out instabilities in the absence of surface roughness. The impact of surface roughness on $\mathcal{H}$ is reflected in the second and third terms of Eq. (5.43), which indicate that the energy dissipation depends on the surface roughness only through an aggregated parameter $A\sqrt{\lambda^{1+k}}$. Hence it is verified once again and quantitatively that rougher surfaces (i.e., with larger A and λ) can induce more energy loss and may increase the work of separation substantially. Another observation from Fig. 9 is that the energy loss decreases monotonically with k. That is, for the same type surface pattern, Gibson solid has the minimum value of the energy loss

among all power-law graded materials. In addition, from the third term in the right hand side of Eq. (5.43), the energy loss is predicted to increase linearly with the incremental amount of contact area from initial contact to the finial loading state. At large indentation depth, a_{im}^2 becomes proportional to δ_{max} according to Eq. (5.26), hence the energy dissipation is a monotonic increasing function of δ_{max}. Similar conclusions about the energy loss for homogeneous isotropic materials were first made by Kesari and Lew (2011).

6. Concluding remarks

In the present paper, the mechanics of axisymmetric adhesive contact of rough surfaces involving power-law graded materials is investigated analytically. A series of general analytical solutions have been obtained with use of the cumulative superposition and equivalent energy release rate approaches for this challenging problem. These solutions provide closed-form expressions of equilibrium relations among applied load, indentation depth and contact radius. Based on these solutions, an effective macroscopic description of the contact evolution is obtained for a general punch profile with surface roughness. Besides the common features as in the case of homogeneous materials, our study reveals that (1) the pull-off force can be influenced by both the gradient exponent k and the modulus variation rate c_0/R of the power-law graded materials, and hence the adhesion strength may be optimized by selecting both the surface topography and the form of material inhomogeneity appropriately. (2) For the considered power-law graded materials, the energy loss during a loading/unloading cycle is controlled by the parameter $A\sqrt{\lambda^{1+k}}$, which indicates that for the same type of surface roughness, the Gibson solid has the smallest value of energy dissipation. Therefore by introducing the power-law graded materials, the toughness of the adhesive contact system can be further improved.

Although the surface roughness is modeled as axisymmetric undulations in the present study, the roughness strengthening, toughening mechanisms and rough-adhesion hysteresis mechanism are expected to be fairly general for both functionally graded and homogeneous elastic solids. Our results may be helpful for understanding of the adhesive contact behavior of systems involving the nonhomogeneous materials with rough surfaces, and the solutions suggests appropriate strategies to improve the interfacial adhesion strength and roughness. Furthermore, the closed-form solution obtained in the paper may also serve as the benchmarks for checking the validity of numerical solution results.

Acknowledgements

The financial supports from the National Natural Science Foundation (10925209, 91216201 and 10932003), 973 Project of China (2010CB832703) and Program for Changjiang Scholars and Innovative Research Team in University (PCSIRT) are gratefully acknowledged. Helpful discussions with Dr. H. Kesari are also gratefully appreciated.

Appendix A: Solution to the generalized Abel integral equation

The generalized Abel integral equation in (3.9) can be converted to

$$\int_0^T \frac{f(a)a\,da}{(T^2-a^2)^{\frac{1-k}{2}}} = \frac{2\cos\frac{k\pi}{2}}{\pi}\int_0^T \frac{a\,da}{(T^2-a^2)^{\frac{1-k}{2}}}\int_0^a \frac{s^k\delta(s)\,ds}{(a^2-s^2)^{\frac{1+k}{2}}}, \qquad (A1)$$

where $T(\geq 0)$ is a variable. Sine $f(r)$ is a continuous and differentiable function of r with $f(0)=0$, after a integration by parts, the left-hand side of Eq. (A1) becomes

$$\int_0^T \frac{f(a)a\,da}{(T^2-a^2)^{\frac{1-k}{2}}} = \frac{1}{1+k}\int_0^T (T^2-a^2)^{\frac{1+k}{2}} f'(a)da\,. \qquad (A2)$$

By reversing the order of integration on the right-hand side of Eq. (A1) and using the identity

$$\int_\beta^\alpha (\alpha-x)^{\frac{k-1}{2}}(x-\beta)^{-\frac{1+k}{2}}dx = \frac{\pi}{\cos(k\pi/2)}, \qquad (A3)$$

we can simplify Eq. (A1) as

$$\frac{1}{1+k}\int_0^T (T^2-a^2)^{\frac{1+k}{2}} f'(a)da = \int_0^T s^k\delta(s)ds\,. \qquad (A4)$$

Differentiating both sides of Eq. (A3) with respect to T results in

$$\delta(T) = T^{1-k}\int_0^T \frac{f'(a)}{(T^2-a^2)^{\frac{1-k}{2}}}da\,. \qquad (A5)$$

Appendix B: Derivation of the asymptotic equilibrium equation

Inserting Eq. (5.12) into the equilibrium $P-\delta$ relation given in Eqs. (5.1)-(5.2) leads to

$$\delta(a) = \delta_M + a^{1-\frac{k}{2}}\Gamma\left(\frac{1+k}{2}\right)\pi^{\frac{2-k}{4}}\lambda^{\frac{k}{2}}\sum_{n=1}^{\infty} n^{1-\frac{k}{2}}\left[-a_n H_{\frac{k}{2}}\left(\frac{2n\pi a}{\lambda}\right) + b_n J_{\frac{k}{2}}\left(\frac{2n\pi a}{\lambda}\right)\right], \quad \text{(B1)}$$

$$P(a) = P_M + \frac{2^{1-k}\vartheta E^*}{(1+k)c_\delta^k}\left[a^2\Gamma\left(\frac{1+k}{2}\right)\pi^{\frac{2-k}{4}}(\lambda a)^{\frac{k}{2}}\Delta_1 - \Gamma\left(\frac{3+k}{2}\right)\pi^{\frac{1-k}{4}}(\lambda a)^{1+\frac{k}{2}}\Delta_2\right], \quad \text{(B2)}$$

where

$$\Delta_1 = \sum_{n=1}^{\infty} n^{1-\frac{k}{2}}\left[-a_n H_{\frac{k}{2}}\left(\frac{2n\pi a}{\lambda}\right) + b_n J_{\frac{k}{2}}\left(\frac{2n\pi a}{\lambda}\right)\right], \quad \text{(B3)}$$

$$\Delta_2 = \sum_{n=1}^{\infty} n^{-\frac{k}{2}}\left[-a_n H_{1+\frac{k}{2}}\left(\frac{2n\pi a}{\lambda}\right) + b_n J_{1+\frac{k}{2}}\left(\frac{2n\pi a}{\lambda}\right)\right]. \quad \text{(B4)}$$

Here H_v and J_v represent the v-th Struve function and v-th Bessel function of the first kind, respectively. In addition, the asymptotic form of H_v can be expressed in terms of Y_v, which is the v-th Bessel function of the second kind, as (Abramowitz and Stegun, 1970, p497, Eq. (12.1.29))

$$H_v\left(\frac{2n\pi a}{\lambda}\right) \sim Y_v\left(\frac{2n\pi a}{\lambda}\right) + \frac{1}{\sqrt{\pi}}\frac{1}{\Gamma\left(\frac{k+1}{2}\right)}\left(\frac{\lambda}{n\pi a}\right)^{1-v} + \mathcal{O}\left(\left(\frac{\lambda}{na}\right)^{3-v}\right),$$

$$\text{as } \lambda/na \to 0. \quad \text{(B5)}$$

In this limit, the Bessel functions J_v and Y_v can also be written in the

asymptotic form as (Abramowitz and Stegun, p364, Eqs. (9.2.1)- (9.2.2))

$$J_\nu\left(\frac{2n\pi a}{\lambda}\right) \sim \sqrt{\frac{\lambda}{n\pi^2 a}}\cos\left(\frac{2n\pi a}{\lambda} - \frac{\nu\pi}{2} - \frac{\pi}{4}\right) + O\left(\frac{\lambda}{na}\right), \qquad \text{(B6)}$$

$$Y_\nu\left(\frac{2n\pi a}{\lambda}\right) \sim \sqrt{\frac{\lambda}{n\pi^2 a}}\sin\left(\frac{2n\pi a}{\lambda} - \frac{\nu\pi}{2} - \frac{\pi}{4}\right) + O\left(\frac{\lambda}{na}\right). \qquad \text{(B7)}$$

Combining Eqs. (B1)-(B7) gives rise to

$$\delta(a) = \delta_L(a) + 2^{\frac{k-1}{2}}\Gamma\left(\frac{1+k}{2}\right)a^{\frac{1-k}{2}}\lambda^{\frac{1+k}{2}}\varsigma\left(\frac{a}{\lambda}\right) + aO\left(\frac{\lambda}{a}\right), \qquad \text{(B8)}$$

$$P(a) = P_L(a) + \frac{2^{\frac{1-k}{2}}\vartheta E^*}{(1+k)c_0^k}\Gamma\left(\frac{1+k}{2}\right)\lambda^{\frac{1+k}{2}}a^{\frac{3+k}{2}}\varsigma\left(\frac{a}{\lambda}\right) + a^2O\left(\frac{\lambda}{a}\right) \qquad \text{(B9)}$$

in the limit of $\lambda/a \to 0$, where

$$\varsigma(\xi) = \sum_{n=1}^{\infty}(2\pi n)^{\frac{1-k}{2}}\left[-a_n\sin\left(2n\pi\xi - \frac{k\pi}{4} - \frac{\pi}{4}\right) + b_n\cos\left(2n\pi\xi - \frac{k\pi}{4} - \frac{\pi}{4}\right)\right],$$

(B10)

Weyl (Zygmund, 1959) defined the α- fractional derivative of a function

$$Q(x) = \sum_{n=1}^{\infty}[a_n\cos(nx) + b_n\sin(nx)] \qquad \text{(B11)}$$

as

$$Q^\alpha(x) = \frac{\mathrm{d}}{\mathrm{d}x}Q_{1-\alpha}(x), \qquad 0 < \alpha < 1, \qquad \text{(B12)}$$

where

$$Q_\alpha(x) = \cos\frac{\pi\alpha}{2}\sum_{n=1}^{\infty}{}' n^{-\alpha}[a_n\cos(nx) + b_n\sin(nx)]$$

$$+ \sin\frac{\pi\alpha}{2}\sum_{n=1}^{\infty}{}' n^{-\alpha}[a_n\sin(nx) - b_n\cos(nx)]. \qquad \text{(B13)}$$

Under this circumstance, it is easy to conclude that $\varsigma(\xi)$ in Eq. (B10) is in fact the

$(1-k)/2$ -fractional derivative of $(f_z(\xi) - a_0/2)$.

References

Abramowitz, M., Stegun, I.A., 1970. Handbook of Mathematical Functions. Dover, New York.

Booker, J.R., Balaam, N.P., Davis, E.H., 1985b. The behavior of an elastic non-homogeneous half-space. Part II. Circular and strip footings. Int. J. Numer. Anal. Methods Geomech. 9, 369–381.

Borodich, F. M., 2008. Hertz type contact problems for power-law shaped bodies. In: Galin, L.A. and Gladwell, G.M.L. eds. Contact Problems: the legacy of L.A. Galin. New York: Springer, pp. 261-292.

Bower, A.F., 2006. Linear Elasticity-Lecture notes. <http:// www.engin.brown.edu/courses/en224/axicontact.html>. Brown University, August, 2006.

Chen, S., Yan, C., Soh, A., 2009a. Adhesive behavior of two-dimensional power-law graded materials. Int. J. Solids Struct. 46, 3398-3404.

Chen, S., Yan, C., Zhang, P., Gao, H., 2009b. Mechanics of adhesive contact on a power-law graded elastic half-space. J. Mech. Phys. Solids 57, 1437-1448.

Derjaguin, B.V., Muller, V.M., Toporov, Y.P., 1975. Effect of contact deformations on the adhesion of particles. J. Colloid Interface Sci. 53, 314–326.

Fuller, K. N. G., Roberts, A.D., 1981. Rubber rolling on rough surfaces. J. Phys. D: Appl. Phys. 14, 100-104.

Fuller, K. N. G., Tabor, D., 1975. The effect of surface roughness on adhesion of elastic solids. Proc. R. Soc. Lond. A 345, 327-342.

Galanov, B.A., 2011. Models of adhesive contact between rough elastic solids. Int. J. of Mech. Sciences, 53, 968-977.

Giannakopoulos, A.E., Suresh, S., 1997. Indentation of solids with gradients in elastic properties: part II. Axisymmetric indentors. Int. J. Solids Struct. 34, 2393–2428.

Goryacheva, I.G., Makhovskaya, Y.Y., 2004. Adhesive Component of the Rolling Friction Force. In: ICTAM04 Proceedings, Warsaw.

Greenwood, J.A., Johnson, K.L., 1981. The mechanics of adhesion of viscoelastic solids. Philos. Mag. A 43, 697-711.

Greenwood, J.A., Williamson, J.B.P., 1966. Contact of nominally flat surfaces. Proc. Roy. Soc. Lond. A 295,300-319.

Guduru, P.R., 2007. Detachment of a rigid solid from an elastic wavy surface: theory, J. Mech. Phys. Solids 55, 445-472.

Guduru, P.R., Bull, C., 2007. Detachment of a rigid solid from an elastic wavy surface: experiment. J. Mech. Phys. Solids 55, 473-488.

Guo, X., Jin, F., Gao H., 2011. Mechanics of non-slipping adhesive contact on a power-law graded elastic half-space. Int. J. Solids Struct. 48, 2565-2575.

Hill, R., Strorakers, B., 1990. A concise treatment of axisymmetric indentation in elasticity. In: Eason, G., Ogden, R.W. (Eds.), Sneddon 70 Anniversary Volume: Elasticity: Mathematical Methods and Application. Ellis Horwood, Chichester, 199-209.

Hui, C.Y., Lin Y.Y., Baney, J.M., Kramer E.J., 2001. The mechanics of contact and adhesion of periodically rough surfaces. J. Polym. Sci., Part B: Polym. Phys. 39, 1195-1214.

Jagota, A., Hui, C.Y., 2011. Adhesion, friction, and compliance of bio-mimetic and bio-inspired structured interfaces. Mater. Sci. Eng. R 72, 253-292.

Jin, F., Guo, X., 2010. Non-slipping adhesive contact of a rigid cylinder on an elastic power-law graded half-space. Int. J. Solids Struct. 47, 1508-1521.

Jin, F., Guo, X., 2012. Mode-mixity-dependent adhesion of power-law graded elastic solids under normal and substrate stretch-induced mismatch strain. Int. J. Solids Struct. 49, 2349-2357.

Jin, F., Guo, X., Zhang, W., 2013. A unified treatment of axisymmetric adhesive contact on a power-law graded elastic half-space. J. Appl. Mech., in press, DOI: 10.1115/1.4023980.

Johnson, K.L., 1985. Contact Mechanics. Cambridge University Press, Cambridge.

Johnson, K.L., 1995. The adhesion of two elastic bodies with slightly wave surfaces. Int. J. Solids Struct. 32, 423-430.

Johnson, K.L., Kendall, K., Roberts, A.D., 1971. Surface energy and the contact of elastic solids. Proc. Roy. Soc. Lond. A 324, 301-313.

Kesari, H., Doll, J., Pruitt, B., Wei, C., Lew, A., 2010. The role of surface roughness during adhesive elastic contact. Philos. Mag. Lett. 90, 891-902.

Kesari, H., Lew, A., 2011. Effective macroscopic adhesive contact behavior induced by small surface roughness. J. Mech. Phys. Solids 59, 2488-2510.

Kim, H.C., Russell, T.P., 2001. Contact of elastic solids with rough surfaces. J. Polym. Sci., Part B, Polym. Phys. 39, 1848-1854.

Li, Q., Kim, K., 2009. Micromechanics of rough surface adhesion: a homogenized projection method. Acta Mech. Solida Sin. 22, 377-390.

Maugis, D., 1992. Adhesion of spheres: The JKR-DMT transition using a Dugdale model. J. Colloid Interface Sci. 150, 243–269.

Maugis, D., 2000. Contact, adhesion and rupture of elastic solids. Springer-Verlag, Berlin.

Morrow, C., Lovell, M.R., Ning, X., 2003. A JKR-DMT transition solution for adhesive rough surface contact. J. Phy. D Appl. Phys. 36, 534-540.

Mossakovskii, V.I., 1963. Compression of elastic bodies under conditions of adhesion (axisymmetric case). J. Appl. Math. Mech. 27, 630-643.

Persson, B.N.J., 2006. Contact mechanics for randomly rough surfaces. Surf. Sci. Rep. 61, 201-227.

Rabinovich, Y.I., Adler, J.J., Ata, A., Singh, R.K., Moudgil, B.M., 2000. Adhesion between nanoscale rough surfaces. I. Role of asperity geometry. J. Colloid Interface Sci. 232, 10-16.

Rvachev, V.L., Protsenko V.S., 1977. Contact problem of elasticity theory for non-classic regions (in Russian). Naukova dumka, Kiev.

Sherge, M., Gorb, S., 2001. Biological Micro- and Nano-Tribology-Nature's Solutions. Springer, Berlin.

Suresh, S., 2001. Graded materials for resistance to contact deformation and damage. Science 292, 2447–2451.

Waters, J.F., Lee, S., Guduru, P.R., 2009. Mechanics of axisymmetric wavy surface adhesion: JKR-DMT transition solution. Int. J. Solids Struct. 46, 1033-1042.

Wei, Z., He, M., Zhao, Y.P., 2010. The effects of roughness on adhesion hysteresis. J. Adhesion Sci. Tech., 24, 1045-1054.

Zappone, B., Rosenberg, K., Israelachvili, J., 2007. Role of nanometer roughness on the adhesion and friction of a rough polymer surface and a molecularly smooth mica surface. Tribol. Lett. 26, 191-201.

Zhuravlev VA. On the question of theoretical justification of the Amontons-Coulomb law for friction of unlubricated surfaces. Proc. IMechE., Part J: J. Eng. Tribol, 221, 893-898.

Zygmund, A., 1959. Trigonometric Series. Cambridge University Press, New York.

Figure captions

Figure 1

A rigid punch with surface roughness is in frictionless adhesive contact with a flat elastically power-law graded half-space under a normal loading P (negative when tensile).

Figure 2

Comparison of the equilibrium $P-\delta$ curves between both rough contact model (black line) and smooth contact model (pink line) for (a) $k=0.1$ and (b) $k=0$. These curves are obtained according to Eqs. (5.8)-(5.11) where the punch profile is specified in Eq. (5.7). The parameters selected here satisfy the simply connected condition in Eq. (2.2).

Figure 3

Actual path of the contact system taken in a displacement controlled loading/unloading process for (a) $P-\delta$, (b) $\delta-a$ and (c) $P-a$ curves, respectively. A complete adhesion and decohesion process is described in these figures with the same set of parameters, and the corresponding points are labeled with the same letter. The actual contact evolution path is only parts of the equilibrium curves (red solid line) combined with unstable jumps at the tip of each corrugation (red dashed line).

Figure 4

Variation of the pull-off force as a function of the wavelength λ. (a) An punch with infinite in-plane size for different values of k; (b) An punch with infinite in-plane size for various values of c_0/R; (c) A truncated punch with different finite

in-plane sizes a_{max} .

Figure 5

Comparison between the equilibrium $P-\delta$ curve (blue dashed line) and its asymptotic form (red solid line) for different values of λ/R, such as (a) 0.1, (b) 0.05 and (c) 0.01. The former is obtained according to Eqs. (5.8)-(5.9) while the latter is plotted according to Eqs. (5.15)-(5.16).

Figure 6

Approximate envelops (green line) of the $P-\delta$ curve and effective contact evolution path at early unloading stage (olive line). These curves are predicted according to Eqs. (5.26)-(5.27) and (5.32), respectively. For comparison purpose, the equilibrium curve (grey line) and the actual path (red line) in Fig. 3a are also included.

Figure 7

Comparison between effective and actual evolutions in a displacement controlled loading/unloading process for (a) $P-\delta$, (b) $\delta-a$ and (c) $P-a$ curves, respectively. The effective evolutions ($P^{\hat{=}}(a^{\hat{=}}_{ep}(\delta))$, $a^{\hat{=}}_{ep}(\delta)$, and $P^{\hat{=}}(a^{\hat{=}}_{ep})$) are labeled in green, while the actual evolutions ($P^{=}(a^{=}(\delta))$, $a^{=}(\delta)$ and $P^{=}(a^{=})$) are labeled in red.

Figure 8

Energy loss in a displacement controlled loading/unloading process. The asymptotic $P-\delta$ curve (grey line) is borrowed from Fig. 4c, and the corresponding effective macroscopic response (green line) including the envelope

of the asymptotic curve and the approximate initial unloading path are obtained according to Eqs. (5.26)-(5.27) and Eq. (5.32), respectively. The complete loading/ unloading cycle is marked by numbers 0-4 and split into two closed path C_1 and C_2 to facilitate the computation of the energy loss.

Figure 9

Energy loss as a function of the gradient exponent k during a loading/unloading cycle. Here, a_{am} represents the approximate maximum contact radius and a_2 is the contact radius at the initial contact.

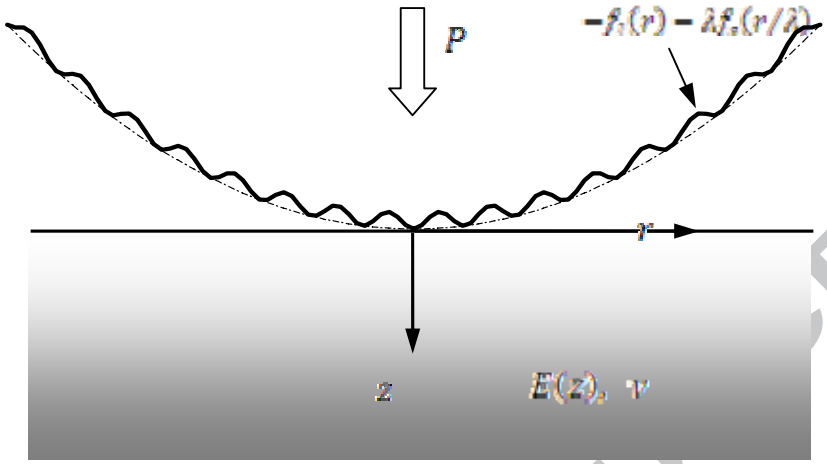

Figure 1

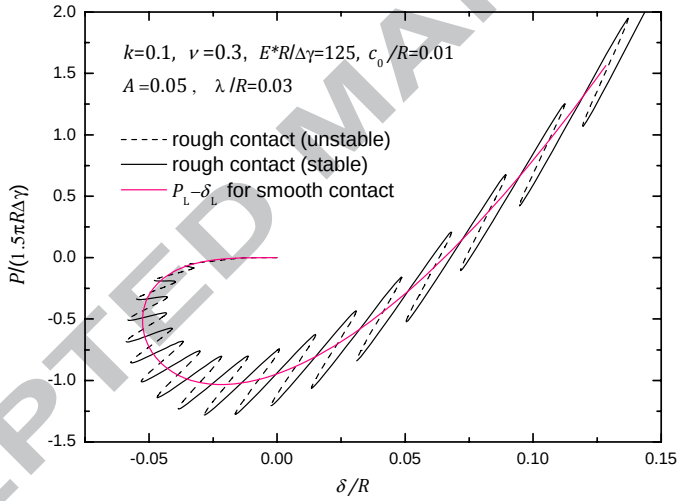

Figure 2a

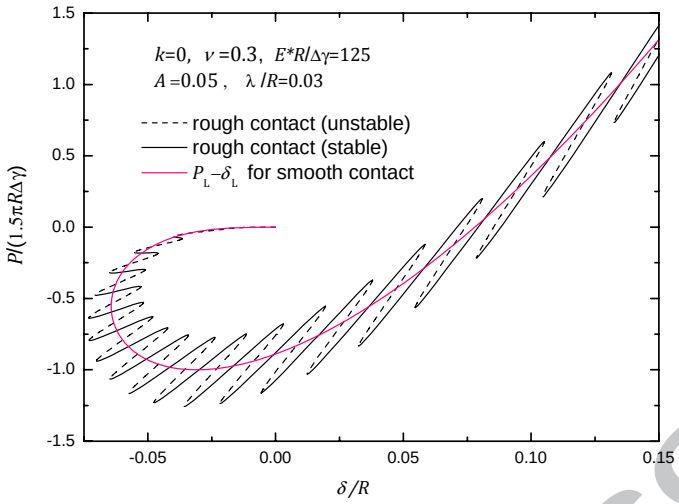

Figure 2b

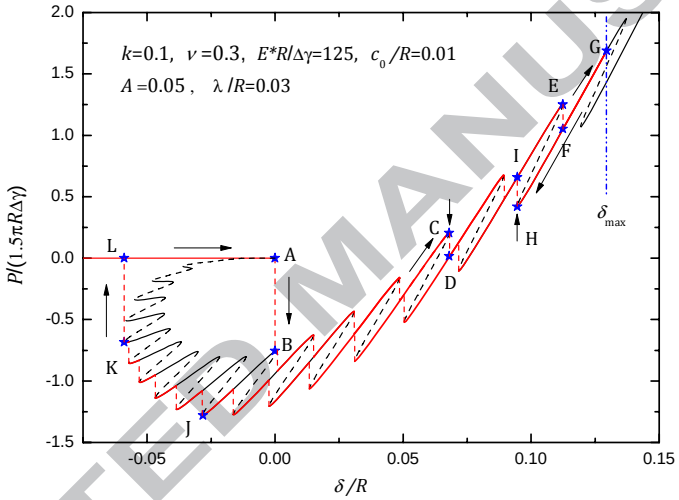

Figure 3a

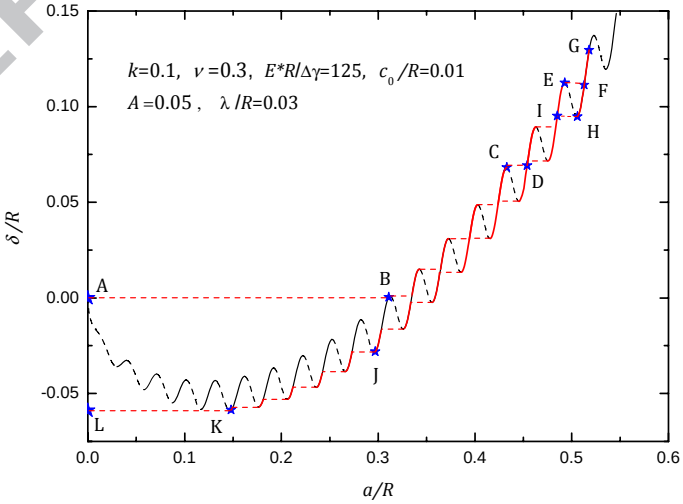

Figure 3b

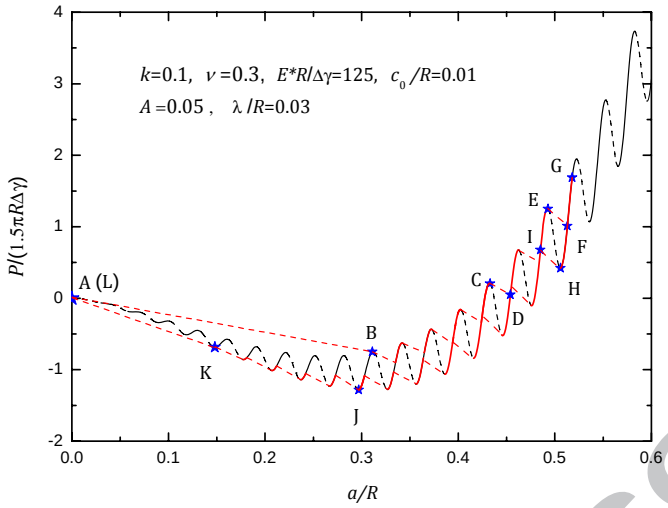

Figure 3c

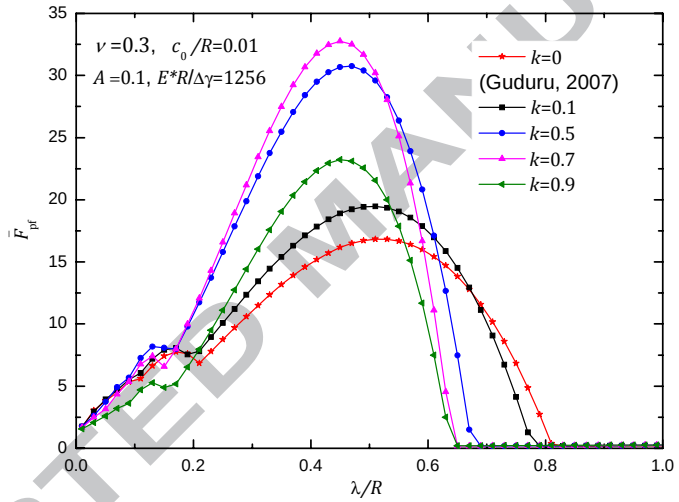

Figure 4a

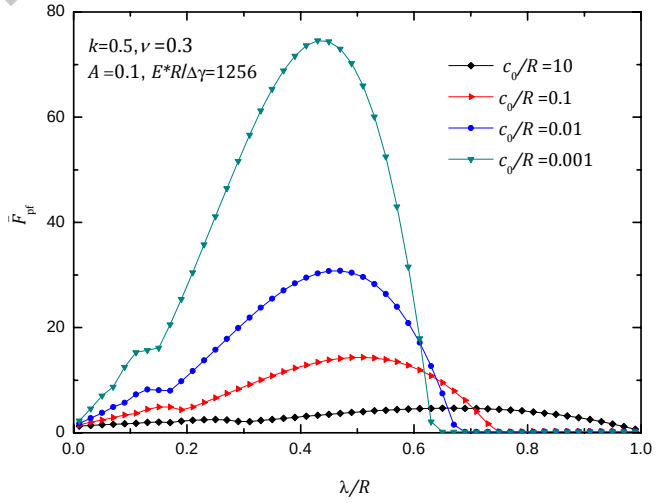

Figure 4b

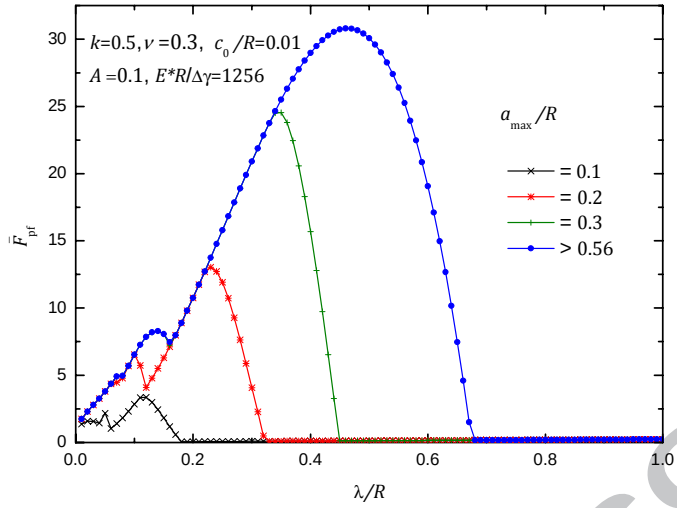

Figure 4c

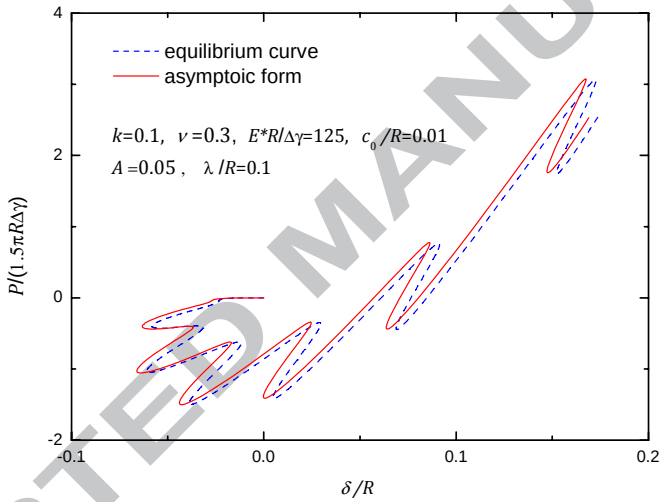

Figure 5a

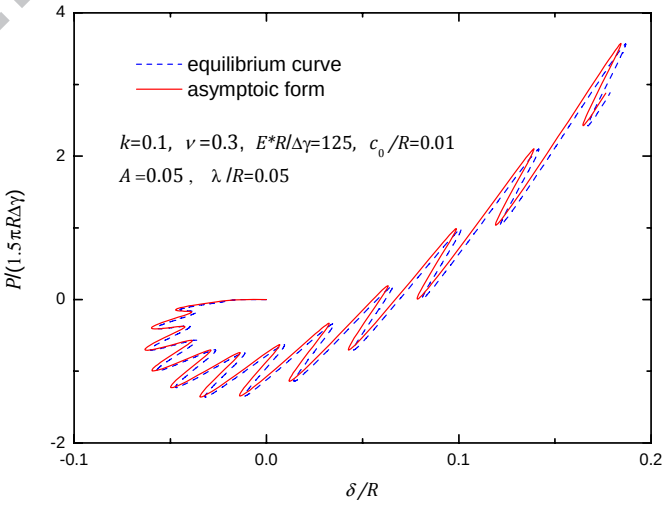

Figure 5b

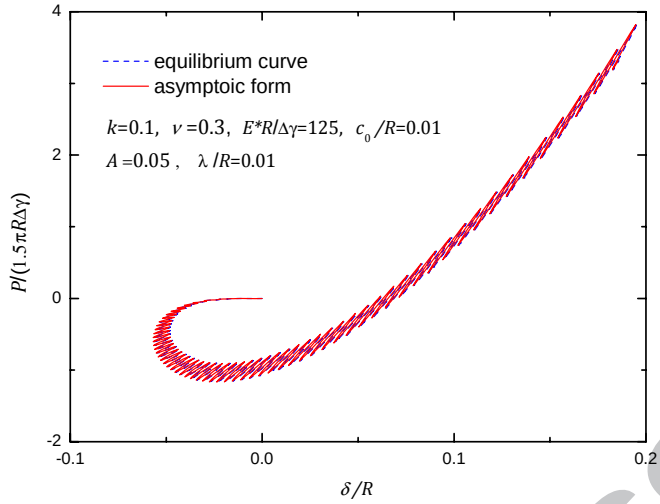

Figure 5c

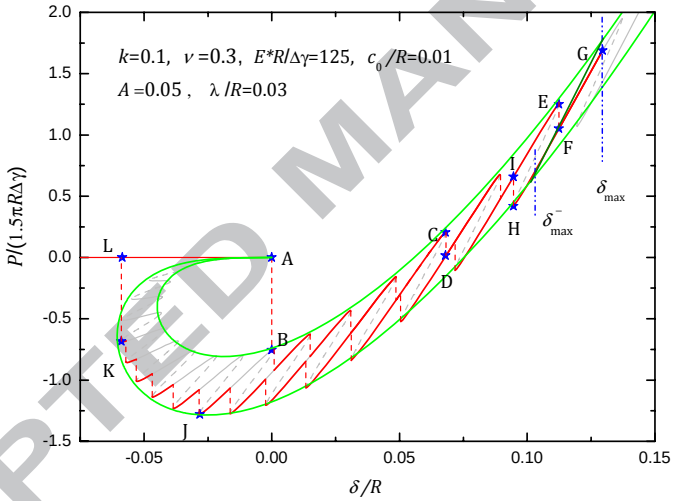

Figure 6

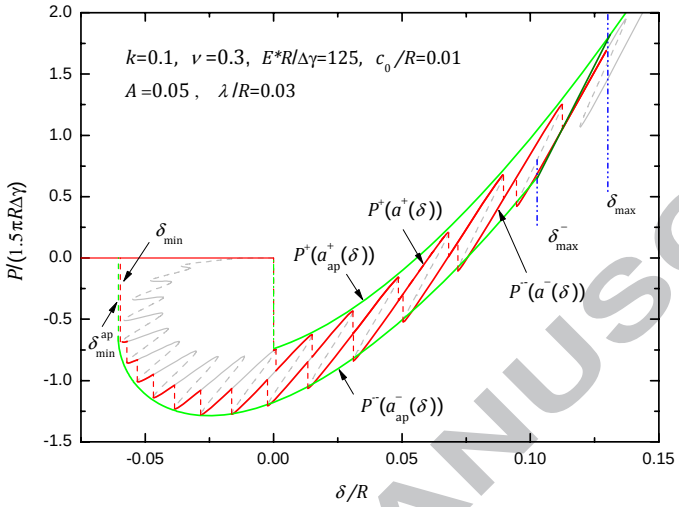

Figure 7a

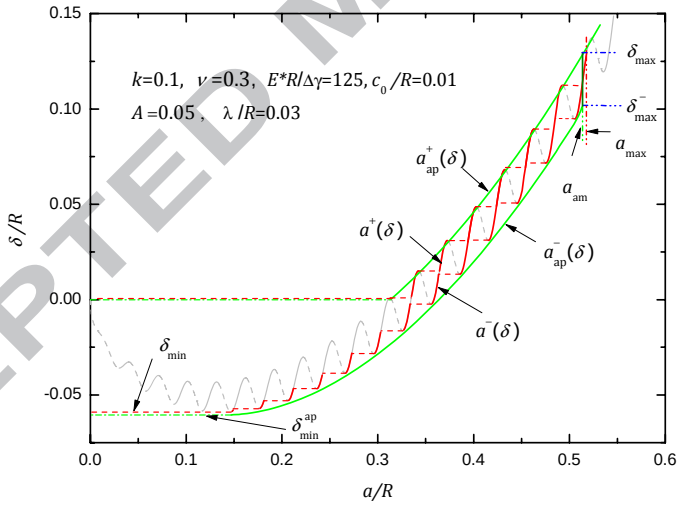

Figure 7b

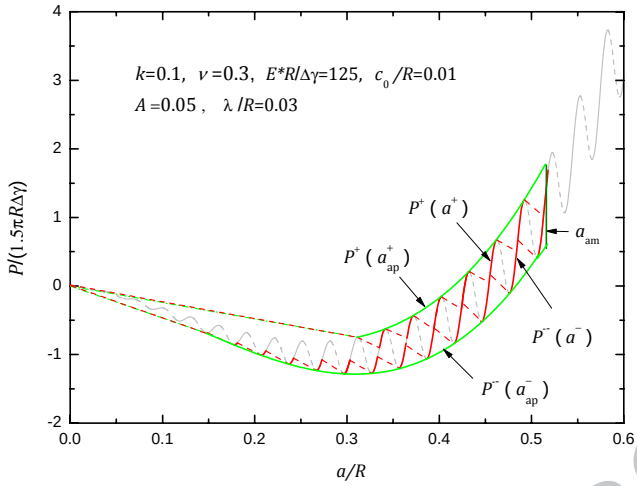

Figure 7c

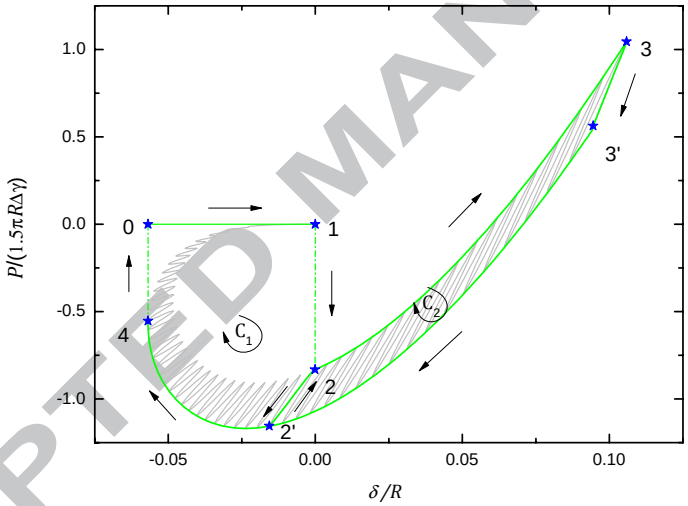

Figure 8

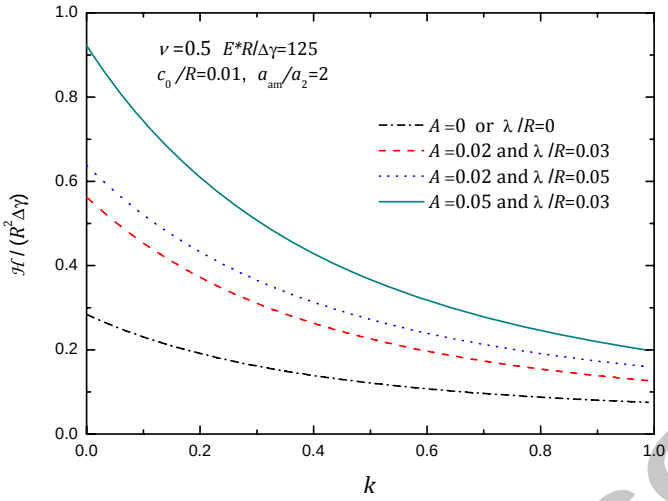

Figure 9